



UNIVERSITÀ  
DEGLI STUDI  
FIRENZE

# FLORE

## Repository istituzionale dell'Università degli Studi di Firenze

### **Energetic optimization of regenerative braking for high speed railway systems**

Questa è la Versione finale referata (Post print/Accepted manuscript) della seguente pubblicazione:

*Original Citation:*

Energetic optimization of regenerative braking for high speed railway systems / Frilli, Amedeo; Meli, Enrico; Nocciolini, Daniele; Pugi, Luca; Rindi, Andrea. - In: ENERGY CONVERSION AND MANAGEMENT. - ISSN 0196-8904. - ELETTRONICO. - (2016), pp. 0-0.

*Availability:*

The webpage <https://hdl.handle.net/2158/1055747> of the repository was last updated on 2021-03-30T14:41:52Z

*Terms of use:*

Open Access

La pubblicazione è resa disponibile sotto le norme e i termini della licenza di deposito, secondo quanto stabilito dalla Policy per l'accesso aperto dell'Università degli Studi di Firenze (<https://www.sba.unifi.it/upload/policy-oa-2016-1.pdf>)

*Publisher copyright claim:*

La data sopra indicata si riferisce all'ultimo aggiornamento della scheda del Repository FloRe - The above-mentioned date refers to the last update of the record in the Institutional Repository FloRe

(Article begins on next page)

# Energetic Optimization of Regenerative Braking for High Speed Railway Systems

---

Amedeo Frilli<sup>1</sup>, Enrico Meli<sup>1</sup>, Daniele Nocciolini<sup>1</sup>, Luca Pugi<sup>1</sup>, Andrea Rindi<sup>1</sup>,

[amedeo.frilli@unifi.it](mailto:amedeo.frilli@unifi.it), [enrico.meli@unifi.it](mailto:enrico.meli@unifi.it), [daniele.nocciolini@unifi.it](mailto:daniele.nocciolini@unifi.it), [luca.pugi@unifi.it](mailto:luca.pugi@unifi.it), [andrea.rindi@unifi.it](mailto:andrea.rindi@unifi.it)

Dept. of Industrial Engineering

University of Florence

Florence, Italy

**Abstract** – The current development trend in the railway field has led to an ever increasing interest for the energetic optimization of railway systems (especially considering the braking phases), with a strong attention to the mutual interactions between the loads represented by railway vehicles and the electrical infrastructure, including all the sub-systems related to distribution and smart energy management such as energy storage systems. In this research work, the authors developed an innovative coupled modelling approach suitable for the analysis of the energetic optimization of railway systems and based on the use of the new object oriented language Matlab-Simscape™, which presents several advantages with respect to conventional modelling tools. The proposed model has been validated considering an Italian Direct Current High-speed line and the High-speed train ETR 1000. Furthermore, the model has been used to perform an efficiency analysis, considering the use of energy storage devices. The results obtained with the developed model show that the use of energy recovery systems in high-speed railway can provide great opportunities of energy savings.

## I. INTRODUCTION

### A. *Energy and Railway Transportation Free Markets and Their Role in a New Green Revolution*

Global Warming and more in general the issues related to pollution are enforcing a growing interest to the increase of efficiency of transportations systems [1], which still represent in Europe and in all industrial countries about 30% of CO<sub>2</sub> pollution sources. This

situation has been investigated by both the Europe Environment Office [2] and the Association of American Railroads [3]; furthermore, Fridell et al. [4] performed a number of experimental tests and found out that, in the railway sector, a significant part of emissions is due to mechanical braking. Railway transportation represents the most efficient technology in terms of pollution and energetic efficiency, but the continuous technological improvements accomplished by its competitors (i.e. ground and air vehicles) are reducing this gap. Furthermore, the current market growth for high-speed and freight sectors in industrialized countries with high population densities would be strongly enhanced by the improvement of the efficiency of the system.

Another important aspect, which is pushing towards a strong energy optimization of the railway system, is the liberalization process of both energy and transportation markets: this process is stimulating all the stakeholders in the railway sector (i.e. energy infrastructures and suppliers, railway infrastructures and vectors) to accurately measure and quantify energy consumptions and their costs. In particular, the combined liberalization of both energy and railway sectors should give to the infrastructure managers the opportunity to apply different costs to traveling trains according to the real measured energy efficiency. Furthermore, the possibility of acquiring energy from different suppliers would allow to optimize costs with respect to the line geographic location, to seasonal factors involving the availability of different resources and, finally, to specific requirements of railway vectors/transport manager. In this scenario, the competition between the different subjects involved in the entire railway field and the need to respect interoperability issues established by the European Railway Agency in the Technical Specifications for interoperability (TSI) [5], will further stimulate the optimization of train energy consumptions, as reported in the analysis of different methods to improve railway energy efficiency performed by Douglas et al. [6].

#### *B. Regenerative Braking and Energy Storage Systems: State of the Art and Literature Review*

In modern railways, aside from the classic considerations that should be made concerning the traction systems and the electrical line, one of the greatest source of energy savings is the use of regenerative braking (see Bartłomiejczyk and Połom [7], who investigated the perspectives of braking energy recovery within urban electrified transports like tramways); in particular, the growing diffusion of trains with distributed traction systems has drastically increased the percentage of energy that can be recovered during the train braking phase. Using regenerative braking instead of the classical dissipative braking allows to convert a relevant part of the train kinetic energy in electric power, without dissipating it over the pneumatic brakes friction surfaces, with another important advantage in terms of brake maintenance costs. Furthermore, the reduced wear and prolonged life of pneumatic brake pads and discs can produce significant benefits in terms of pollution, since the brakes wear produce solid particles and contaminants whose impact on the environment is still a matter

of monitoring and research: Abbasi et al. [8] analysed the particles due to brake wear and proposed a comparison index to identify their impact, Gehrig et al. [9] performed experimental tests in a Switzerland railway node and Salma et al. [10] performed their experimental analyses on polluting particles near Budapest.

The application of regenerative braking involve the availability of a load or a storage device (whose performances in electric vehicles have been investigated by Marr et al. [11]) able to manage the energy recovered from the braking phase of the train: Hillmansen et al. [12] found that a significant percentage of the railway energy consumption could be saved using proper storage devices.

The peak power  $W_{max}$  that has to be managed during regenerative braking is roughly proportional to the maximum speed reached by the train before braking  $v_{max}$ , to the deceleration of the train during the braking phase  $a_{brk}$  and to the train equivalent inertia  $m_t$ , which takes into account also the contributions to kinetic energy due to motors, gearboxes, axles, wheels and brake discs.

On the other hand, the mean power  $W_{mean}$  that can be regenerated depends on the kinetic energy of the train  $m_t v_{max}^2$  and on the braking occurrence  $f_b$  (i.e. defined as the number of braking events with respect to traveling time). On tramways and light urban railways, the vehicles traveling speed and equivalent inertia are much smaller with respect to high-speed trains, but the braking frequency  $f_b$  is much higher: therefore, the mean regenerated power  $W_{mean}$  is relatively high with respect to the peak power  $W_{max}$ . For this reason, the power management of regenerative braking is typically easier on tramways, metro and light urban railways with respect to high-speed lines. Furthermore, the length of metro and tramway lines is typically lower than conventional lines: hence it is easier to implement customized innovative solutions (e.g. the synchronization of trains accelerations and decelerations, investigated by Peña-Alcaraz et al. [13]). Consequently, the application of energy storage systems on metro, tramways and more in general on light railway systems has been widely recognized as an important opportunity for energy optimization and has been extensively investigated by different authors, while the application of energy recovery systems in high-speed trains is still an open research field: Falvo et al. analysed the energy efficiency of a metro system, comparing a Spanish and an Italian line [14] and González-Gil et al. [15] investigated the most important energy savings possibilities in urban railway.

Research works available in literature can be typically classified as follows:

- Energy storage systems location: energy storage systems can be stationary or installed on board the vehicle. Barrero et al. [16] investigated the advantages and disadvantages of on-board and stationary energy storage devices, using a simulation tool to analyse the metro line of Brussels, while Teymourfar et al. [17] investigated the use of stationary supercapacitors within the Tehran metro network. The on-board configuration allows to reduce electrical line losses and assures system autonomy even with bad or

discontinued current collection. On the other hand, stationary systems connected to the infrastructure are easier to install and maintain, avoiding additional weights and encumbrances on vehicle, which can penalize performances and available payload for goods and passengers.

- Energy storage systems application and usage: the most typically analysed applications are tramways or metro, where energy storage systems allow to save energy, reduce line voltage fluctuations and optimize both energy and infrastructure costs. In particular, Teymourfar et al. [18] analysed the possibility to perform energy recovery within a metro network, Ceraolo and Lutzemberger [19], using the Modelica™ environment, analysed and compared different configurations useful to increase the efficiency of tramways, Barrero et al. [20] analyzed the energetic efficiency of light railways, investigated the sizing of Ultra-Capacitors for the Brussels tramway [21] and performed an analysis on a set of on-board supercapacitors for a tram, evaluating also the effect of power converter (Barrero et al. [22] and Van Mierlo et al. [23]), while González-Gil et al. [24], [25] analysed different strategies to enhance the energetic efficiency of urban railway systems, including regenerative braking. Furthermore, Iannuzzi et al. [26] proposed a technique to optimize the sizing of ultracapacitors for light railways and Mir et al. [27] designed a supercapacitor storage system for tramways. The shortage of research works concerning energy recovery in high-speed railway applications represents an important lack, which should be filled in order to enhance the efficiency of the entire railway system.
- Energy storage technology: Vasebi et al. [28] developed an innovative method for the calculation of batteries State Of Charge, which is fundamental for the correct analysis of batteries behaviour; Tsang et al. [29] proposed and validated a model for the analysis of Li-ion batteries (which are the most suitable for the use in the railway field), as well as Castano et al. [30]; on the contrary Zhu et al. [31] analysed the use of Pb-acid batteries for energy storage purposes. Other researchers have studied batteries behaviour considering their use together with other storage devices, like Trovão and Antunes [32], who investigated the possibilities to use a hybrid storage systems coupling batteries and supercapacitors, or with fuel cell-powered systems, like Guo et al. [33], who analysed the use of batteries in a fuel cell-powered locomotive (the batteries are able to store braking energy and to cover transient energy requests), Paladini et al. [34], who investigated the use of both on-board batteries and supercapacitors in a fuel cell-powered vehicle, developing a Matlab-Simulink™ model (the use of Matlab-Simulink™ is typical in the analysis of this kind of systems), and Thiounn-Guermeur [35], who developed a hybrid locomotive which uses two different storage systems. Supercapacitors are relatively new with respect to batteries, but it is possible to find in literature many studies concerning their behaviour, like that by Sharma and Bhatti [36], where they proposed a detailed analysis of the characteristics of supercapacitors and of their applications, or that by Steiner et al. [37], where they analysed the use of on-board ultracapacitors. Among the many possibilities to implement

energy storage, researchers have analysed the different performances that a device could provide in different systems; an important work is that by Kondoh et al. [38], who performed a comparison of different energy storage systems, highlighting which technology could better suit specific applications. Finally, for a correct use of energy storage devices it is fundamental to be aware of the subsystems needed for their operation (see Fernão Pires et al. [39], who analysed the power electronics devices needed by different energy storage systems to be successfully employed in electrical systems) and also to understand the complete life cycle of the considered device; an important analysis of this last point is provided in a work by Oliveira et al. [40], where they investigated the environmental characteristics of energy storage devices, taking into account their whole life cycle. Current energy storage technologies differ in terms of costs, specific energy and power densities. Therefore, the design and sizing of these systems (and of regenerative braking systems themselves) are influenced by the adopted storage technology, especially for on-board applications where the installation of energy storage systems is limited by interoperability issues and by weight and encumbrance constraints.

### *C. Application of Object Oriented Modelling Languages to Simulation Models*

Most of the previously cited research works analyse (in terms of simulation, design and optimization) the use of energy storage systems in railway applications through simulation models developed to reproduce the following aspects:

- An accurate simulation of the railway vehicle longitudinal dynamics with a particular attention to power balances, especially during traction and braking phases.
- An electrical model of the overhead electrical line able to reproduce the effects of catenary and sub-stations equivalent impedance according to the line topology and to the relative positions of the loads represented by traveling trains.

In order to understand the feasibility of energy storage systems, a wide variety of different simulation scenarios should be analysed; furthermore, a high level of customization is needed to adapt models to different kind of railway vehicles, line layouts and operating conditions. Models should adopt a parametric approach to perform a large number of simulations and customized blocks must allow to be easily assembled by users with different levels of skill.

Due to these reasons, the usage of high level languages is mandatory and often proposed in more recent works: Fernandez et al. developed a Matlab-Simulink™ model of an electric power system for tramways [41], Uzunoglu et al. [42] used the Matlab-Simulink™ environment, coupled with the SimPowerSystems™ tool, to analyse the behaviour of a hybrid ultracapacitor system, and Hannan et al. [43] developed a Matlab-Simulink™ control system for the management of the energy sources in electric vehicles.

127 In particular, Pugi [44] and Conti [45] in recent works adopted a modular architecture based on Matlab-Simulink™, which is the current  
128 standard for the simulation of dynamical systems and the prototyping of applications involving control, diagnostic and signal processing.  
129 One of the limits of a pure Matlab-Simulink™ architecture such as that proposed in [44] and [45] is represented by the modelling  
130 compromises that have to be introduced to preserve code modularity and numerical efficiency.

131 In particular, redundant integrated state are often added to the model in order to reduce algebraic loop or solve implicit algebraic  
132 relationship, with significant losses also in terms of accuracy.

133 More recent object oriented languages like Modelica™ [19] or Matlab-Simscape™ allow the user to describe the response of a  
134 component in terms of balance equations, following an approach which clearly resemble the Bond-Graph one (approach also followed  
135 by Ramakrishnan et al. [46] for the analysis of the dynamical behaviour of mechatronics systems).

136 In particular, Matlab-Simscape™ allows the modelling of physical system through a lumped parameters approach, considering the  
137 constitutive equations of each element of the system: while a Matlab-Simulink™ block receives an input and, based on the mathematical  
138 operations implemented within itself, provides an output, a Matlab-Simscape™ block contributes to the complete model through a set  
139 of ordinary or differential equations. The complete system is then solved applying a symbolic approach. The Matlab-Simscape™  
140 environment has a series of built-in physical domain, each containing a large set of the elements usually employed in lumped parameters  
141 modelling. Furthermore, it is possible to develop custom domains and blocks written in the Matlab-Simscape™ programming language.  
142 A Matlab-Simscape™ model handles physical variables, considering also their units of measurement, while a Matlab-Simulink™ model  
143 only handles numerical signals; however the two environments can be completely connected, coupling blocks developed in both ways.  
144 The main advantages of this innovative approach can be summarized as follows:

- 145 • Optimization of the number of integrated states: the balance equations of each component are symbolically pre-processed in order  
146 to minimize the number of integrated states, avoiding the usage of redundant auxiliary states; this increases the numerical efficiency  
147 of the model and reduces the memory consumption without losses of accuracy.
- 148 • Bidirectional correspondence between the model topology and the modelled physical system: the elements of the model are  
149 implemented in terms of physical balances with respect to an assigned set of variables which depends on the specific definition of  
150 the considered physical domain (e.g. mechanical and electrical). Therefore, a single line graphical link between sub-models is  
151 automatically associated to a bidirectional exchange of variables that reproduces the physical interactions of the modelled physical  
152 network. This feature provides important benefits in terms of modularity, simplicity and ease of use.

#### 153 *D. General Architecture of the Proposed Model*

154 With respect to the current state of the art summarized in the previous paragraphs, in this work the authors propose an innovative  
155 modelling approach useful to deal with the following aspects:

- 156 • The application of energy storage systems to high-speed railways.
- 157 • The use of the object oriented environment Matlab-Simscape™, with a particular attention to real time implementation and to  
158 distributed computing.

159 Energy recovery in high-speed trains is a quite new field of analysis, because the advantages deriving from this application are harder  
160 to achieve with respect to light railway systems; the braking frequency and the energy involved in the manoeuvre in high-speed railway  
161 systems are not optimal to use the same solutions found in light railways, hence a deep analysis is needed to fully understand the possible  
162 recovery perspectives. The potential energy recovery in this sector is significant, and an accurate analysis could lead to identify how to  
163 exploit it.

164 Furthermore, the use of the innovative Matlab-Simscape™ language allows to obtain accurate results with a great numerical efficiency,  
165 providing the possibility to perform a large number of simulations and investigate many different scenarios. This feature is essential to  
166 be able to perform an energetic optimization of the system.

167 In order to correctly analyse the energetic prospects of the considered railway systems, the proposed model has also been experimentally  
168 validated.

#### 169 II. MATERIALS AND METHODS

170 The developed model is composed of the following sub-systems:

- 171 • Dynamical model of the vehicle;
- 172 • Electrical model of the line;
- 173 • Multi-Model Mission Planner for complex line topologies and multi-vehicle simulations.

174 In the following Sections, the authors will expose the main features of the elements of the proposed model, to highlight the novelty of  
175 the approach and introduce the results obtained with the model. Furthermore, the real operating scenario considered as a test case will  
176 be exposed.



## 177 A. Dynamical Model of the Vehicle

178 The mechanical behaviour of the train is modelled using a simplified lumped parameters approach [47]. The model is developed using  
 179 the Matlab-Simulink™ environment coupled with a series of object oriented Matlab-Simscape™ blocks.

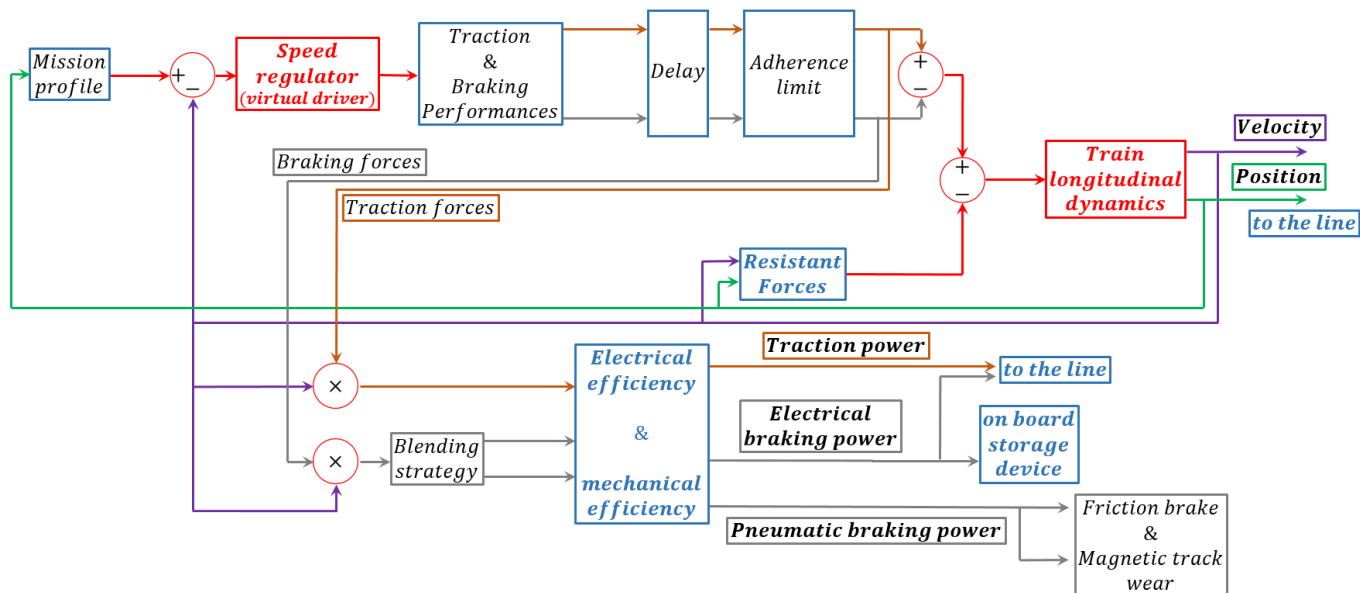


Figure 1: Architecture of the vehicle dynamical model.

Figure 1 shows the general architecture of the mechanical sub-model: the user can impose a position-based mission profile and, through the comparison with the current velocity of the vehicle, a virtual driver regulates the traction or braking requests. These forces are dynamically applied and properly saturated considering adherence limits. The calculation of the train motion takes into account both traction and braking forces and various resistant loads. Traction and braking forces and the vehicle velocity are then used to calculate the requested or provided power, taking into account a blending strategy chosen by the user and the electrical and mechanical efficiency of the system. This model provides to the electrical part the train position and the electrical traction and braking power; the pneumatic braking power can be used to estimate the wear of the braking system.

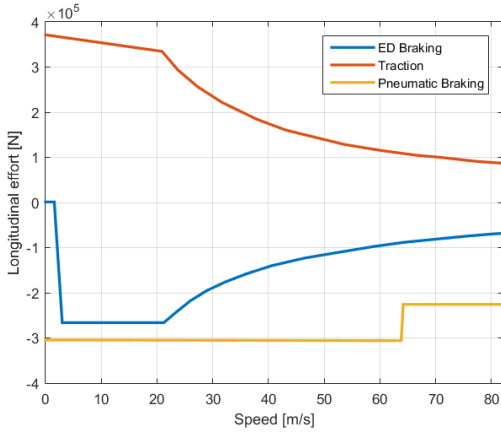


Figure 2: Traction and Braking Performances of ETR 1000 High-speed Train (referred to a 3kV DC line).

The longitudinal dynamics of the vehicle can be analysed according to the following Equation of motion:

$$m_i \ddot{x} = T - mg \sin a - m(a\dot{x} + b\dot{x}^2 + c + d(r)), \quad (1)$$

where  $m_i$  is the mass of the vehicle,  $x$  is the position of the train within the line,  $a(x)$  is the slope of the line,  $a$ ,  $b$ ,  $c$ ,  $d(r)$  are equivalent coefficients used to calculate motion resistances as a function of speed ( $a, b$ ), internal frictions of the train ( $c$ ), and additional resistances ( $d(r)$ ) due to curves with radius  $r(x)$ , and  $T$  represents the total longitudinal forces applied by traction or braking system.

The maximum longitudinal forces applied in the traction and braking phases are calculated according to tabulated relationships which depend on the train speed and reproduce the curves reported in Figure 2.

Both traction and braking forces are applied with a smoothed dynamics obtained with a first order filter that reproduces the typical limitations introduced on both systems to improve the longitudinal comfort of the passengers and protect the train from excessive mechanical solicitations. The corresponding numerical implementation in terms of gradient/slew rate of both traction and braking forces is described in Table 1.

Further saturations are introduced in order to reproduce the effect of the limited wheel-rail adhesion along the line; in particular, the traction force  $T_T$  and the braking one  $T_B$ , which can be exerted as a function of the available adhesion  $\mu$ , are calculated according to Equations (2) and (3):

$$T_T \leq T_{T_{\max}} = k_m m g \mu, \quad (2)$$

$$T_B^3 T_{B\max} = - m g m. \quad (3)$$

The coefficient  $k_m$  is defined as the ratio between the vertical load on motorized axis and the total weight of the train; for the ETR 1000 the value of this coefficient is about 0.5.

The value of the wheel-rail adhesion  $\mu$  is calculated taking into account the dependency of the available adhesion on the vehicle speed:

$$m = \frac{m_0}{1 + k_{muller} \cdot \frac{v}{kmh}}, \quad (4)$$

where  $m_0$  is the static value of the friction factor, which typically varies between 0.35 and 0.4,  $\frac{v}{kmh}$  is the train speed in km/h and

$K_{muller}$  is a scaling parameter which ranges between 0.005 and 0.011.

As reported in Figure 3, it should be noticed that the wheel-rail adhesion predicted according to Equation (4) in a speed range between 200 and 350 km/h for a value of  $K_{muller}$  equal to 0.0065 is quite similar to the available adhesion prescribed by TSI regulations for the design of braking systems.

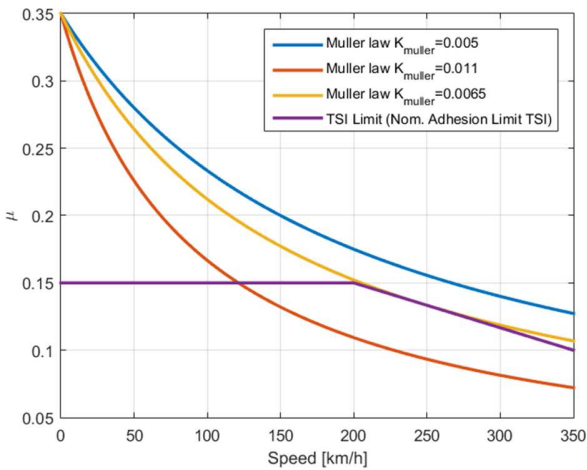
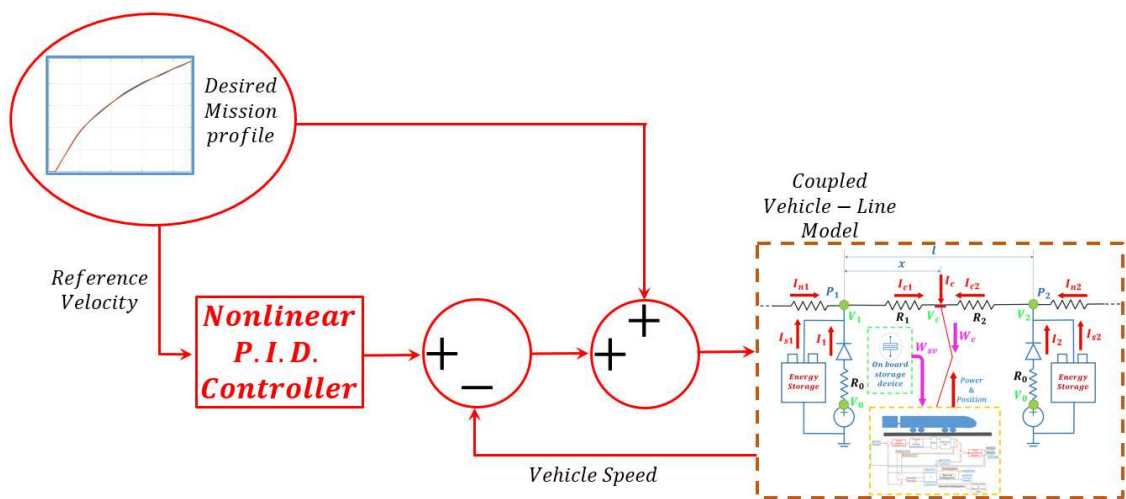


Figure 3: Wheel-Rail Adhesion as a function of the vehicle speed: comparison between the Muller Model and TSI limits.

Traction and braking manoeuvres are calculated with respect to an assigned speed profile through a PID regulator, which acts on the difference between the desired velocity and the current train velocity; this regulator has been developed in a previous version of the model [45]. The proposed control strategy (shown in Figure 4) is quite simple. The speed regulator is used to calculate the traction and braking forces needed to drive the train respecting the desired speed profile. The desired speed profile could be influenced by the line

222 layout, by the timetable and by the signalling system. The virtual driver should represent the action of the human driver: hence the P.I.D.  
 223 controller has been developed to act with a low dynamics and to tolerate velocity errors of about 2 m/s.

224



225 *Figure 4: Scheme of the virtual driver implemented in the proposed model.*

226 This control strategy has been chosen for its simplicity; however, in the future developments of the model, some optimization techniques  
 227 will be used to improve the efficiency and accuracy of the controller.

228

229 *Table 1: Dynamical response of High-speed Trains braking and traction systems.*

Braking Application	4[s] to apply the full braking effort from the brake released condition
Braking Release	12[s] to completely release the brake from a full braking condition
Traction Application	7[s] to apply the full traction effort from a null traction condition
Traction Release	Traction is immediately deactivated without any appreciable delay

230

After the calculation of the longitudinal effort  $T$ , it is possible to determine the train speed by integrating its acceleration (calculated according to Equation (1)); it is then possible to calculate the mechanical power  $W_m$  delivered to the vehicle by the traction system as follows:

$$W_m = T \cdot v \quad (5)$$

During the braking phase, both the traction system and the conventional brake cooperate to dissipate the kinetic energy of the train; thus, a part of the mechanical power  $W_m$  (denoted as  $W_{mb}$ ) is dissipated by the pneumatic brake, while the remaining part (denoted as  $W_e$ ) is converted in electrical power by the traction system itself.

The converted power  $W_e$  can be dissipated on on-board resistors (dissipative braking) or transferred to be stored or reused (regenerative braking). The management strategy of the different braking systems during the braking phase is usually called blending (see Leigh [48] for a review of railway braking systems and their interactions). In this research work, the authors have considered a blending criterion that in normal operating conditions maximizes  $W_e$  against  $W_{mb}$  (according to the maximum performance curves reported in Figure 2).

It is possible to define a conversion efficiency  $\eta_{tot}$  as follows:

$$h_{tot}(T, v) = h_e h_m \begin{cases} W_m > 0 \Rightarrow h_{tot} = \frac{W_m}{W_e} \\ W_m < 0 \Rightarrow h_{tot} = \frac{W_e}{W_m} \end{cases} \quad (6)$$

Equation (6) expresses the proportionality between the mechanical power  $W_m$  and the corresponding electrical power  $W_e$ , which can be absorbed (traction phase) or regenerated (braking phase) by the traction system.  $\eta_{tot}$  can also be expressed as the product of the mechanical efficiency of mechanical transmission system  $\eta_m$  and the electrical efficiency  $\eta_e$  of on-board traction equipment. The efficiency  $\eta_{tot}$  is typically a function of both train speed and delivered traction effort.

In case of regenerative braking, the recovered power  $W_e$  can be divided in two terms: a first part, denoted as  $W_c$ , is transferred to the line and a second one, indicated by  $W_{sv}$ , is stored on a possible on-board accumulator (described in Section II.B). In order to simulate the power consumption of additional on-board auxiliary systems, a further contribution,  $W_{aux}$ , must be introduced. The complete power balance between those contributions due to the different on-board sub-systems is reported in Figure 5 and can be expressed as follows:

$$W_e = W_{aux} + W_{sv} + W_c \quad (7)$$

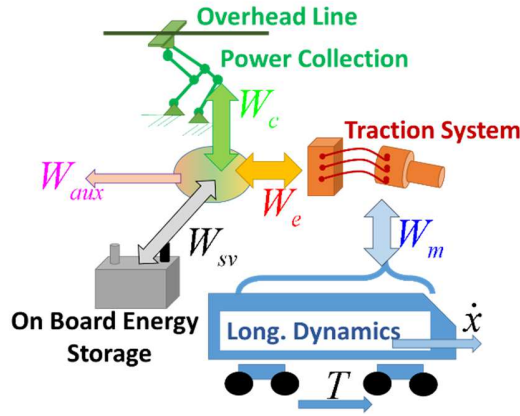


Figure 5: Power fluxes involved in the vehicle dynamics, considering the interactions with the electrical line.

It is important to underline that, to properly calculate the power  $W_c$  collected by the train, it is fundamental to take into account the line slope  $\alpha$  and additional resistance  $d(r)$  due to curves (which are defined as tabulated functions of the position  $x$  of the train) for each line section, since the line resistance can provide a significant portion of power losses. The power  $W_c$  calculated through this Equation is then used as an input to the line and hence to the stationary energy storage devices present within the line.

#### B. Electrical Model of the Line

Figure 6 shows a scheme of the architecture of the electrical line model: the proposed model has been developed using both standard and custom Matlab-Simscape™ and includes the contact line, the electrical substations, stationary and on-board storage devices. The model exchanges with the mechanical part the vehicle power and position.

The considered line is a 3kV DC catenary which is bilaterally fed by two Electrical Sub-Stations (ESSs), modelled as ideal voltage generators with an equivalent impedance and a diode (to simulate the first quadrant limitation of the system) connected in series; ESSs are often analysed with similar models in literature works (see the books written by Perticaroli [49] and Zaninelli [50] on railway electrification systems). In this configuration the sub-station is able to provide only traction power, while a possible recovered braking power could only be used by another train within the line. This scenario is consistent with the considered test case (see Section II.D); however the model is able to represent also the fourth-quadrant behaviour of the line. A simple solution is based on the use of energy storage devices: the fourth quadrant operation is handled directly by those devices, which can receive the braking energy and provide part of this power when the same vehicle or another one needs traction power. Furthermore, the fourth quadrant operation can be also

modelled by using fully reversible substations (see Section III.D), able both to provide and receive energy; this solution has been considered also by Cornic [51], who analysed the possibility to perform energy recovery through a reversible sub-station. For the considered application (i.e. a high-speed line), the mean distance between adjacent ESSs is about 15 km, hence the presence of two trains in the same line section should be considered uncommon, taking into account that the signalling system for a vehicle speed of about 200-250km/h imposes a minimal distance of 5400 m from the nearest protected point. Furthermore, in order to fully exploit its maximum speed (up to 360km/h for the considered test case), the safety distance between the train and a protected point should be at least twice or even three times the minimal value because the braking distances are roughly proportional to the squared value of the vehicle speed.

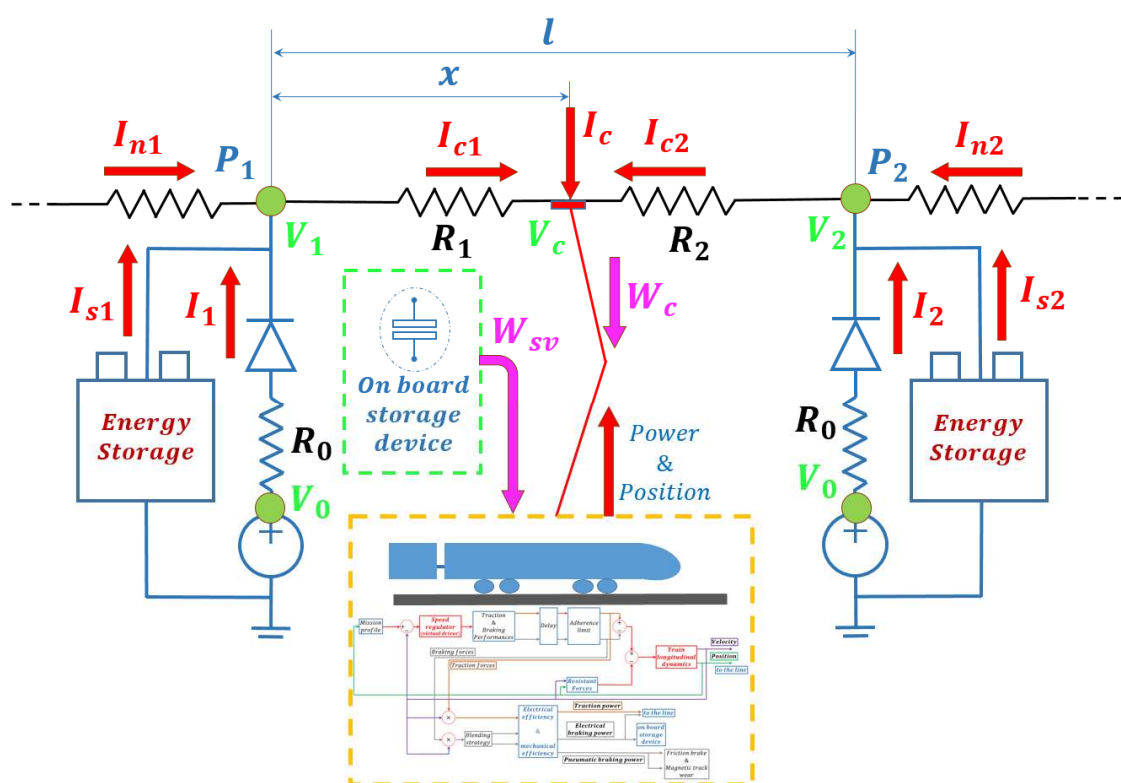


Figure 6: Architecture of the electrical line model, including stationary and on-board energy storage devices.

The power  $W_c$ , collected by the train in correspondence of the pantograph and hence calculated by the vehicle sub-model described in the previous Section, is provided as an input to the electrical model of the line. Figure 6 shows the architecture of the feeding line in a generic instant of the train operation while Figure 7 shows the model couplings during regenerative braking: the power provided by the train can be received by stationary or on-board energy storage devices.

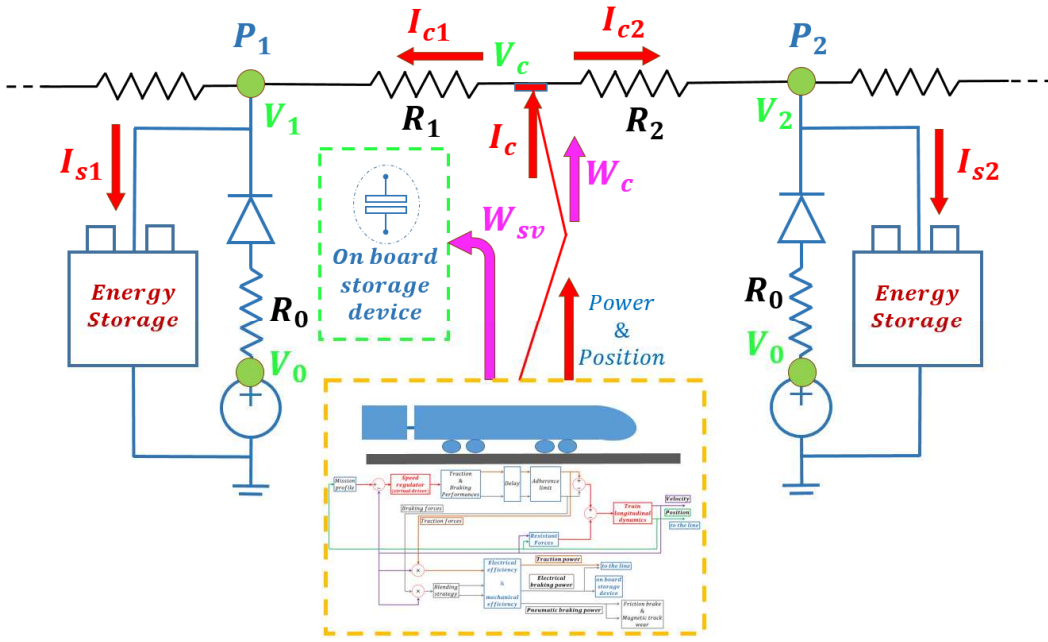


Figure 7: Architecture of the electrical part of the model during regenerative braking.

In order to couple the mechanical and the electrical parts, it has been necessary to introduce a delay in the variable exchange between the vehicle dynamics and the feeding line. However, since the goal of the proposed model is the analysis of the train energy consumption, it is not necessary to examine the high frequency components and the various harmonics present within the line. Hence, the presence of a time delay (needed for the model coupling), has no influence on the analysis and does not destabilize the system because the time scale considered in the simulations are much higher than the considered delay. The integration time step used is about 5 seconds.

The vehicle virtually divides each line section in two parts, whose impedance values depend on the train position; the equivalent resistances  $R_1$  and  $R_2$  of those catenary sections are calculated as a function of the train position  $x$  with respect to the distance  $l$  between adjacent sub-stations, according to Equations (8) and (9):

$$R_1 = (1 - d) \times R_{tot}, \quad (8)$$

$$R_2 = d \times R_{tot}, \quad (9)$$

$$d = \frac{P_2 - x}{l}, \quad (10)$$

where  $P_2$  is the position of the next substation and  $R_{tot}$  is the resistance of the complete line section included between the two considered substations.



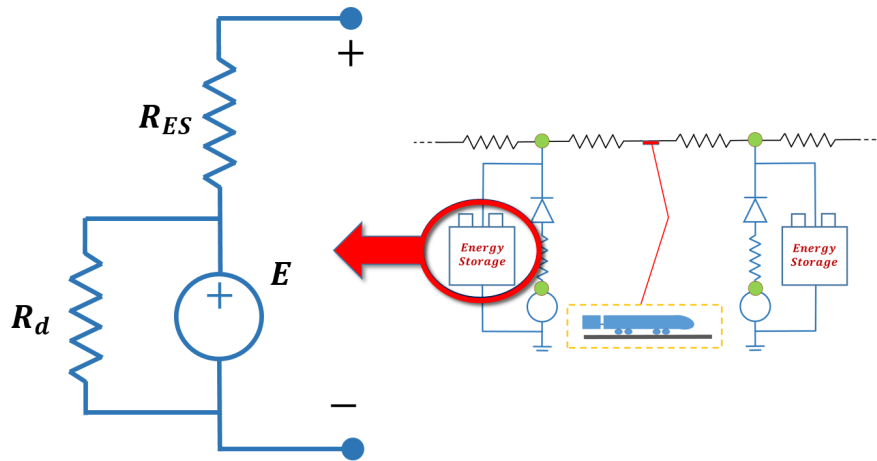


Figure 8: Scheme of the energy storage device model.

The most common stationary energy storage devices are batteries and supercapacitors: in this research work, the authors have chosen a basic modelling approach suitable for both the systems. The proposed energy storage device model (shown in Figure 8) is a load connected in parallel to the ESSs and includes an ideal voltage generator, a resistance in parallel with the voltage source to simulate the device transient discharge and finally a resistance in series.

This quite simple modelling approach allows to correctly simulate the behaviour of batteries and supercapacitors while requiring only a limited set of parameters to work. Furthermore, this energy storage device, thanks to the characteristics of the object oriented language used for the development of the model, can be easily connected or disconnected to ESSs, providing the possibility to simulate a large number of operating scenarios and to optimize the distribution of the devices themselves with respect to the energetic efficiency of the system. Finally, this simple model can be used also to represent a capacitor employed as an on-board storage device (useful in tramways and light railways or to cut down voltage peaks during regenerative braking). This modelling approach can be extended to the approximated modelling of complex energy storage systems in which the accumulator is coupled to the line through a two quadrant converter like the one reported in Figure 9.

Furthermore, in order to be able to investigate more deeply the specific physical behaviour of the storage devices, the authors have also started to develop a more complex battery model.

The architecture of the battery model is shown in Figure 10: in this specific model the resistance  $R_{ES}$  is substituted by the series of a resistance  $R_o$  and a parallel between a further resistance  $R_l$  and a capacitor  $C$ . These further elements allows to better analyse the transient behaviour of the device (while the resistance  $R_d$  takes into account self- discharge phenomena). The voltage of the ideal voltage generator

is calculated through the estimation of the battery S.O.C.: the value  $E$  of the no load tension of the storage system is a tabulated function of the energy storage device current  $I_m$  and of the state of charge of the device. The S.O.C. is an auxiliary state used to characterize the storage device and can be defined as follows:

$$S.O.C. = \int \frac{h_I(I_m, S.O.C.) I_m}{E_{max}} dt \quad (11)$$

where  $h_I$  is the efficiency of the device, i.e. a tabulated function of both  $I_m$  and S.O.C., and  $E_{max}$  is the maximum stored energy. Different kind of accumulators can be easily represented and their internal losses can be analysed in terms of impedances or efficiency  $h_I$ .

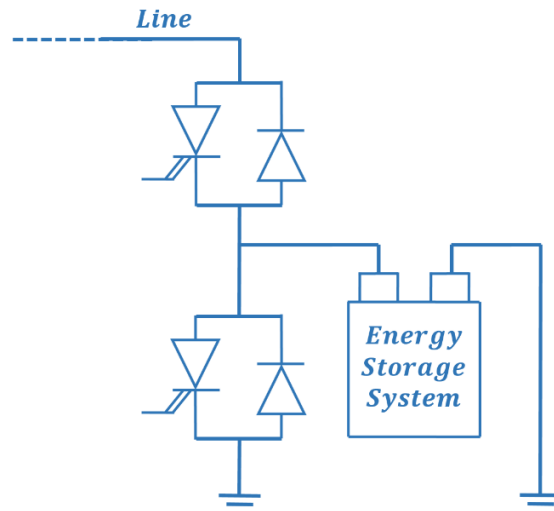


Figure 9: Scheme of an energy storage device connected to the line through a two quadrant converter.

The authors chose to investigate the behaviour of Li-ion batteries, which could better suit to the needs of railway systems. The battery size has been determined starting from a reference Li-ion cell with a nominal voltage equal to 3.7 V and a nominal capacity of 53 Ah. In order to reach the line voltage, the entire battery includes stacks of 1000 cells connected in series (considering an intermediate value of the S.O.C.); 4 stacks are then connected in parallel to obtain the desired capacity. In particular, the capacity of the entire battery, in order to assure a long life to the device, has been determined considering the maximum recovered braking energy (or the maximum provided traction energy) to be about 5-10% of the full battery capacity.

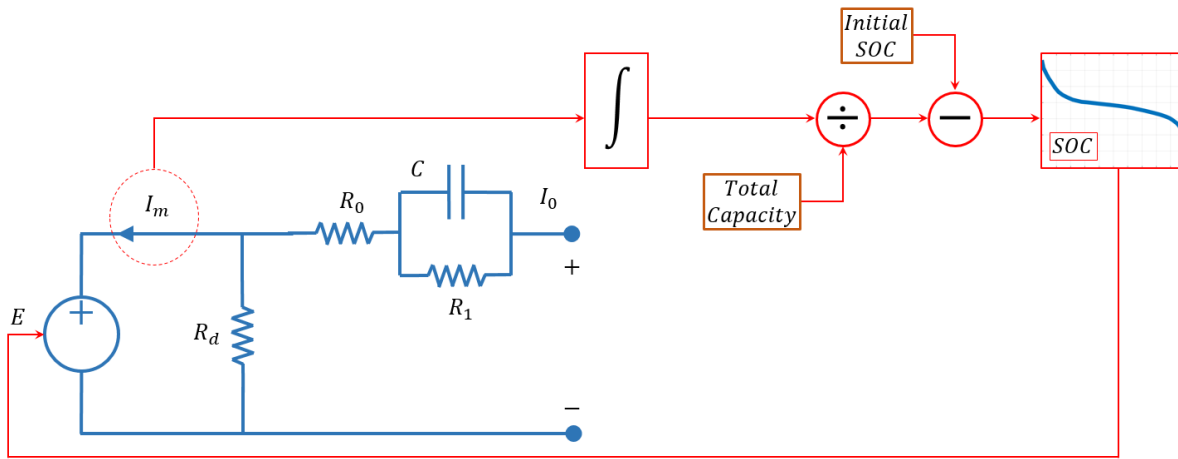


Figure 10: Scheme of the battery model, including the S.O.C. calculation.

Figure 11 and Figure 12 show respectively the charge and discharge behaviour of a battery with the previously exposed characteristics. The discharge behaviour shown in Figure 12 highlights the voltage variation as a function of the S.O.C.: the trend is quite steep, however, considering the small percentage of energy represented by a braking manoeuvre with respect to the entire battery capacity, the voltage variations about the nominal value can be considered acceptable. In this operating range the current is constant during the charge phase. These results have been obtained simulating the behaviour of the battery connected with a load (i.e. a current generator in the charge phase and a resistance in the discharge phase).

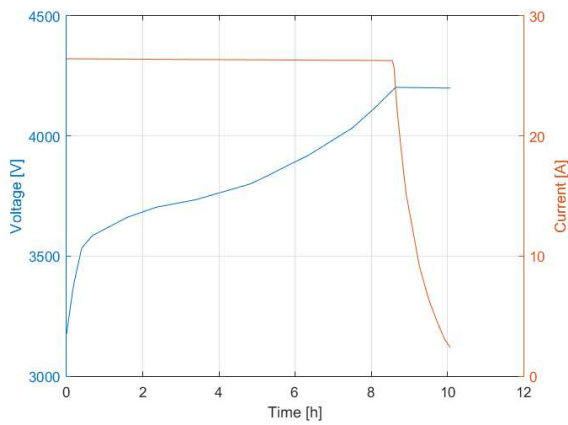


Figure 11: Battery charge behaviour.

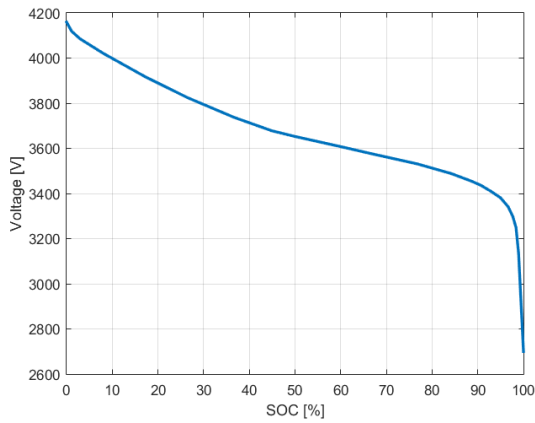


Figure 12: Battery discharge behaviour.

In order to obtain realistic results concerning the battery behaviour within the line, a good approach to connect this battery model to the proposed coupled model is to use an initial S.O.C. equal to about 50%, to work within the nominal range of the battery even with the maximum possible depth of discharge due to the passage of an accelerating train.

Currently the State Of Health (S.O.H.) of the battery is not taken into account; each battery is considered fresh. This is due to the large number of data needed to correctly model battery aging. Furthermore, the life expected from the batteries sized as previously exposed is about ten years; hence, for the analysis of the possible savings due to train regenerative braking, it is not fundamental to consider this aspect. However, in order to analyse the use within a railway system of second-hand batteries (e.g. recovered from electric cars), in a future release of the model the estimation of the S.O.H. will be implemented.

In this research work this quite complex battery model has not been used yet; in fact the authors have preferred to start their analyses considering a simplified scenario.

Complex topology lines with more than a single section, like the one shown in Figure 13, can be easily assembled because it is possible to connect to line nodes additional loads or section lines (corresponding to the external currents  $I_{n1}$  and  $I_{n2}$  shown in Figure 6).

By solving the electrical network it is possible to calculate the train collected current  $I_c$  and all the other currents involved in the operation of the line sub-components.

### C. Multi-Model Mission Planner

As reported in the example shown in Figure 13, it is possible to assemble models considering even more than one traveling train on the line. The authors have developed a GUI (Graphical User Interface) to facilitate the assembly of complex topology system; this GUI is

denoted as Multi-Model Mission Planner. Through the Multi-Model Mission Planner it is possible to associate to each train model a pattern corresponding to the train mission; in particular, the mission profile is defined by the variables  $t_{ref}$ ,  $x_{ref}$ , and  $p_{ref}$  described in Table 2.

The Multi-Model Mission Planner is able to switch the loads corresponding to different traveling trains along the line according to a precise timeline imposed by the user.

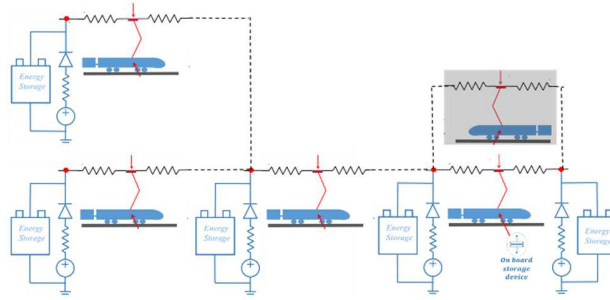


Figure 13: Example of complex line topology: the presence of intersections and multiple vehicles increases the complexity of the system but also the possibilities in terms of energy optimization.

Table 2: Variables needed by Multi-Model Mission Planner.

$t_{ref}$	Time sequence associated with mission events.
$x_{ref}$	Sequence of the longitudinal positions of the train along the line defined with respect to the time vector $t_{ref}$ . From $x_{ref}$ it is also possible to calculate the desired speed profile for the vehicle and the arrival and departure times from simulated stations
$p_{ref}$	Sequence of sections that the train should occupy during the missions; it is fundamental to simulate switches and complex topologies.

#### D. Considered Test Case: ETR 1000 on the Firenze-Roma Line

In this research work, the authors consider, for the validation of the proposed model, a high-speed train with the characteristics of the ETR 1000, the last high-speed train developed for Trenitalia by Bombardier and AnsaldoBreda (AnsaldoBreda Group has now been purchased by Hitachi).

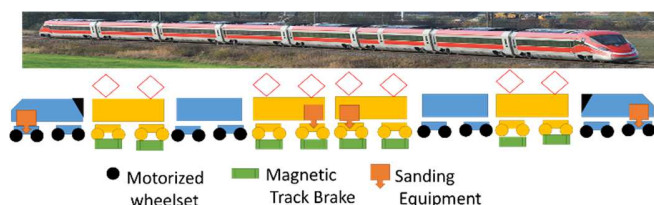
The main technical features of the considered train are listed in Table 3; the vehicle has a distributed traction system, shown in Figure 14, whose traction and braking performances are shown in Figure 2 (real operating scenario).

Currently the ETR 1000 is in a preliminary homologation and testing phase, so the data described in this paper, which are mainly referred to the preliminary presentations of the train (see the technical specifications of the train [52] and the paper by Gherardi and Vannelli [53], who analysed interoperability issues between European High-speed trains) could be subjected to slight modifications due to the final calibration and optimization of on board systems. The most interesting reference is represented by the proceedings of a CIFI (acronym for Collegio degli Ingegneri Ferroviari Italiani) Symposium [54], a conference where the participation of many train suppliers made possible a deeper insight on train functionalities and performances.

Table 3: Main features of the train of the ETR1000 High-speed Train.

Total Seats	About 470
Carbody Construction	Aluminium Alloy
Train Mass	500 [t]
Train length	202 [m]
Axle Load	17 [t]
Gauge	Standard 1435 [mm]
Rotating Inertia respect to train mass	4 %
Wheel diameter	920 [mm]
UIC classification	Bo'Bo'+2'2'+Bo'Bo'+2'2'+2'2'+Bo'Bo'+2'2'+Bo'Bo'
Motorized Weight Fraction	0.5 [-]
Traction system	Water-cooled IGBT Converters and Asynchronous AC Traction Motors
Supported Electrification Standards	25 kV 50 Hz, 15 kV 16.7 Hz, 3 kV DC, 1.5 kV DC
Nominal Power	9.8 [MW]
Max Tractive Effort (standstill)	370 [kN]
Nominal Speed	75 [km/h]
Max Speed (design)	400 [km/h]
Max Speed (commercial)	360 [km/h]
Acceleration / Dec. Performances	0.7 [ms <sup>-2</sup> ] (acc.) / 1.2 [ms <sup>-2</sup> ] (dec.)
Braking system	Electro-Pneumatic, Electric Braking (both regenerative or dissipative), Magnetic Track Brake
Brake Pad Consumption	0.1-0.2 [cm <sup>3</sup> /MJ] (depending on installed brake pad and demanded brake power)

389 The ETR 1000 is designed to operate under different electrification standards: thus it is able to respect interoperability standards among  
 390 the most important railway networks of western Europe.  
 391 In particular, in this research work the authors consider the operation of the ETR 1000 within the 3kV DC Firenze-Roma line (usually  
 392 denoted as “Direttissima”), which is the oldest and perhaps more important high-speed line of the Italian network. Figure 15 and Table  
 393 4 show the main electrical features of the considered line.



394  
 395 *Figure 14: Distributed traction and braking systems of the ETR 1000 High-speed Train.*

396 The ETR 1000 traction system can be used in a regenerative braking configuration; however, the energy recovery is currently limited  
 397 by the availability of a load along the electrical line. In fact, the Electrical Sub-Stations currently installed along the “Direttissima” line  
 398 are designed to operate only in the first quadrant: they are not fully reversible substations and there are no stationary energy storage  
 399 devices within the line. Furthermore, in order to protect the line from potentially harmful overvoltage, the train switch from regenerative  
 400 to dissipative braking if the line overvoltage exceeds a value of about 3900 V.



401  
 402 *Figure 15: Catenary of the Firenze-Roma “Direttissima” High-speed Line.*

403 In this work, the authors investigate the feasibility and the potential advantages of the application of energy storage technologies to  
 404 high-speed trains, to understand how to fully exploit the regenerative braking capabilities of those trains. The considered high-speed

test case has been used both for the experimental validation of the proposed modelling approach and for the energy recovery feasibility analysis.

Table 4: Main (approximated) electrical features of the “Direttissima” High-speed Line.

Line Impedance ( $r$ )	About 0.05 [Ohm/km]
ESS No Load Voltage	3700 [V]
ESS EQ. Impedance	About 0,09 [Ohm]
Mean Distance between ESSs	14.7 [km]
Min Distance between ESSs	12 [km]
Max Distance between ESSs	16.8 [km]

### III. RESULTS AND DISCUSSION

ETR 1000 is a relatively new project and currently represents one of the most relevant investment performed by the Italian railways. During the drawing up of this research work, the train was still performing its preliminary experimental activities on Italian high-speed lines; consequently, it was hard to find available data for the validation of the model. The data available for the preliminary validation of the proposed model were referred to a specific manoeuvre performed during the train homologation phase: during the preliminary homologation process the train has been subjected also to experimental tests concerning high frequency measurements of collected currents and voltages (the frequency ranges from 20 kHz to 200 kHz). These tests were not performed to evaluate the train efficiency; their goal is the evaluation of the harmonic contents of collected currents and voltages: this analysis is useful to understand various problems related to train power collection and concerning power drives, on-board filters and the quality of pantograph current collection. In order to make those data usable for their scientific purposes, the authors have filtered and down-sampled them to obtain smooth profiles useful for their analysis but with almost no industrial interest, since the information about high frequency behaviour is completely lost (the authors considered a maximum sampling frequency of 10 Hz).

The authors aim to prove the accuracy of the results provided by the proposed model and its ability to reproduce a real high-speed operating scenario through the comparison with those data and not to perform an exact evaluation of the parameters needed to set the wage that the vehicle must pay to use the feeding line.

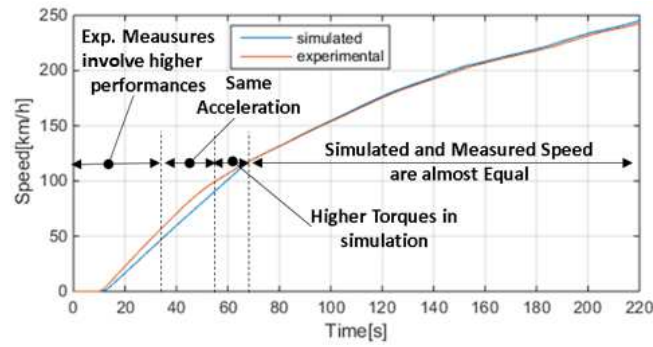


In this Section, for the experimental validation of the proposed coupled vehicle-line model, the authors used a set of experimental data concerning a specific traction manoeuvre of the ETR 1000 on the high-speed line Roma-Firenze, from standstill to a speed equal to 250 km/h. The manoeuvre is performed applying the maximum traction effort corresponding to the curves shown in Figure 2. Figure 16 shows the comparison between the measured vehicle speed profile and that obtained with proposed model: it is possible to verify that the main parameters considered in the model concerning traction performances, inertia and motion resistances were substantially correct. In particular, the numerical and experimental speed profiles above 110 km/h are almost identical (with negligible errors both in terms of speed and acceleration). Below 110 km/h there are some differences between the two profiles; in particular, the real train exhibits higher performances. This error has to be carefully evaluated considering real adhesion conditions and axles skidding phenomena. Axle skidding phenomenon is strictly connected to the adherence of the track: during the traction phase it is identified as slipping, while during the braking phase it is denoted as sliding. In both cases the phenomenon is due to a difference between the wheelset velocity and the speed of the vehicle itself (e.g. the wheel locking during braking) and it leads to a vehicle skidding. Axle skidding can be dangerous in terms of safety; furthermore, it is important to avoid it in order to prevent excessive wheel and track wear. Train traction performances used in the proposed model are perhaps a bit lower than the real ones since they are referred to a continuous guaranteed performance; at the same time, it should be noticed that maximum performances near to standstill conditions involve the availability of an adhesion which is higher than 0.15, which is the limit usually adopted for the design of braking systems according to TSI standards. TSI limits are cautious because they are referred to the braking sub-system, which is quite safe relevant. However, considering the Muller adhesion model shown in Figure 3, it has to be observed that with a vehicle speed above 85 km/h the maximum expected adhesion limit is lower than 0.25. Consequently, in the speed range between 80 and 120 km/h there is a high statistical occurrence of skidding. As a matter of fact, during the experimental tests some skidding occurs in this speed range, confirming that the maximum performances of the system are a bit higher than those assumed within the proposed model but they cannot be fully reached in the most common operating conditions without causing the intervention of anti-skidding systems. The implementation of an anti-skidding sub-model in the proposed model could allow to better represent the train behaviour observed experimentally during the complete traction phase.

The aim of this first comparison is to validate the proposed model in a real operating scenario, to verify its reliability before using it to analyse the feasibility of energy recovery systems within the system.

In particular, the authors focused their attention on the calibration of the set of parameters described in Table 5, which were affected by larger uncertainties.

452 However, it is important to notice that the uncertainties on these quantities have almost no influence on the controller used to drive the  
 453 vehicle. This is due to the need to represent the behaviour of the human driver: the velocity errors are higher and the dynamics of the  
 454 intervention are slower than those of an automatic driver. Hence, in terms of controller effectiveness, the uncertainty on the model  
 455 parameters are almost completely compensated by the approximation of the controller itself.



456  
 457 Figure 16: Comparison between a real traction manoeuvre on the Firenze-Roma High-speed Line and the corresponding numerical results obtained  
 458 with the proposed model.

459  
 460 Table 5: Model uncertain parameters that should be further identified and refined.

Uncertain Parameter	Reason/comments
Train efficiency $\eta_t$	This parameter is affected by heavy uncertainties concerning both the mechanical efficiency $\eta_m$ of the transmission system and the electrical one $\eta_e$ . In addition, the heavy uncertainties on motion resistances can be partially compensated adjusting $\eta_t$ .
Pos. of power connections along the line $l$	The positions of power stations are well known but the positions of the electrical connections along the line are affected by errors of about 50m.
ESSs voltage and impedance $V_0, R_0$	These parameters have to be further investigated.
Equivalent resistivity of the line $\rho$	This parameter has to be further investigated.

461

#### 462 A. *Identification and Validation of the Efficiency $\eta_t$*

463 The comparison between the experimental and numerical power consumption can be analysed in Figure 17. The test begins with a phase  
464 in which the train is stopped and its motors are not working. In this phase, which corresponds to the first 10 seconds of the experimental  
465 record, it is possible to measure the small power flux that must be collected from the line to feed all the auxiliary systems of the train.  
466 It is not a very accurate measurement; however, a constant power  $W_{aux}$  equal to about 230 kW seems to be a realistic approximation,  
467 because it corresponds to a mean consumption of about 23 kW for each wagon. This power flux is needed for the operation of air  
468 conditioning, lights, and every on-board sub-system such as compressors for pneumatic brakes and battery chargers.  
469 Furthermore, by comparing the collected power  $W_c$  provided by the proposed model with that experimentally measured, it is possible  
470 to perform a calibration of the train global efficiency  $\eta_t$ ; the results of this preliminary calibration are reported in Table 6. Within the  
471 proposed model,  $\eta_t$  is taken into account after the dynamical analysis of the vehicle, in correspondence of the power consumption  
472 calculation: this value of  $W_c$  takes into account both the chosen blending strategy and the system global efficiency. Considering that the  
473 dynamical part of the model produces results in good agreement with the experimental measurements (e.g. in terms of velocity profile,  
474 see Figure 16), and that there is no blending since the considered manoeuvre includes only a traction phase, all the possible errors in  
475 terms of power consumption can be attributed to the erroneous value of the global efficiency. Then, the comparison between  
476 experimental and numerical  $W_c$  allows to tune the value of  $\eta_t$ . In the proposed model, due to lack of more detailed experimental  
477 measurements,  $\eta_t$  is assumed to depend only on the vehicle speed, neglecting the dependency on the traction effort. However, it should  
478 be noticed that the mechanical efficiency of the transmission systems typically increases as the transmitted power increases while the  
479 efficiency of power electronics components is typically higher for partial loads. Consequently, the mutual compensations of these  
480 phenomena should produce a reduced fluctuation of the global efficiency around its most common value, which is about 0.84.  
481 Finally, it is possible to highlight that the efficiency value equal to 0.82 calculated in the speed range between 40 and 120 km/h is a bit  
482 low due to the axle skidding phenomenon: in fact it produces rapid transients and hysteretic load cycles which penalize the global  
483 efficiency of the system.

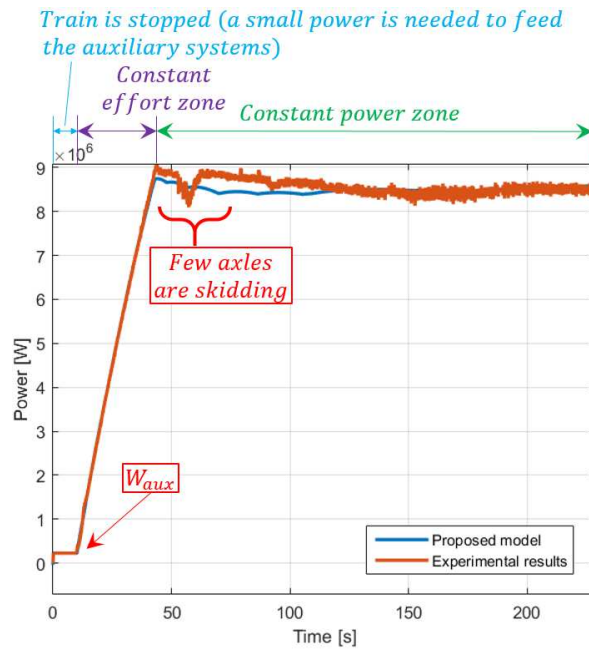


Figure 17: Comparison between the experimental power consumption  $W_e$  during the traction phase and the corresponding numerical values obtained with the proposed model.

Table 6: Preliminary calculation of the global efficiency  $\eta_t$  with 100% of the traction effort applied.

Speed Range	Global efficiency $\eta_t$ at 100% of the traction effort
0-36 [km/h]	From 0.8 to 0.82
36-54 [km/h]	0.82
54-126 [km/h]	From 0.82 to 0.86
126-162 [km/h]	0.86
162-180 [km/h]	From 0.86 to 0.85
180-236 [km/h]	0.85
236-350 [km/h]	From 0.85 to 0.83

#### B. Identification and Validation of Power Station Parameters

After a preliminary evaluation of the traction system efficiency, it is possible to refine some parameters related to the electrical line. This analysis concerns the identification of the position, the no-load voltage and the equivalent impedance of the power stations within the line starting from the measurements of the voltage  $V_c$  in correspondence of the pantograph, which are reported in Figure 18.

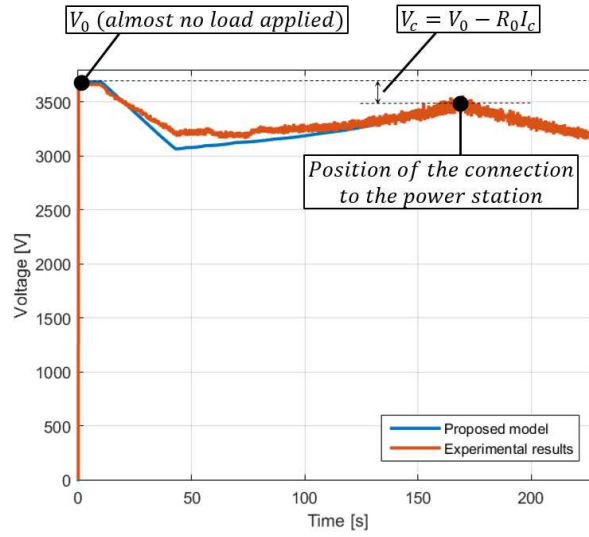


Figure 18: Comparison between the line voltage  $V_c$  experimentally measured at the pantograph during the traction phase and the corresponding numerical values obtained with the proposed model.

In particular, it is possible to calculate and verify the value of the sub-stations no-load voltage  $V_0$  by considering the measured voltage in correspondence of the standstill condition: in this case the collected power is small and causes negligible losses; hence the measured voltage in correspondence of the pantograph can be assumed to be equal to  $V_0$ .

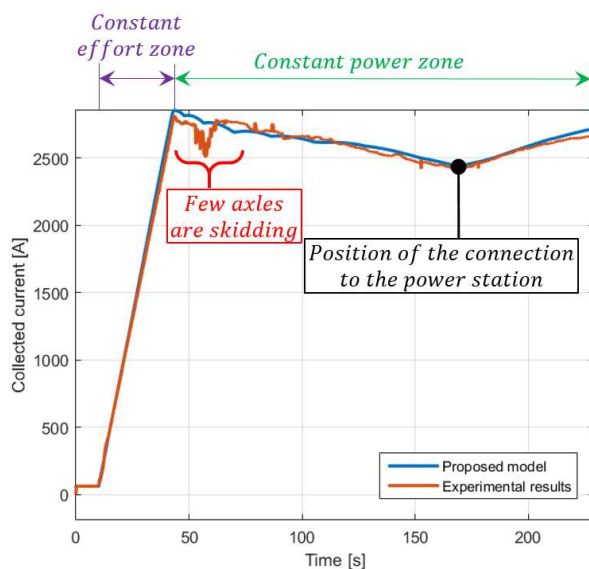
Furthermore, the position of the power connection can be refined (within the data uncertainty of about 50 m) considering that the passage under a power connection in a constant power operating condition (see Figure 17) produces a peak in the pantograph measured voltage  $V_c$  (shown in Figure 18). In this case, almost all the power needed by the train is collected locally. Consequently, the line circuit behaviour can be analysed through Equation (12) and the linearized equivalent impedance of the electrical sub-station  $R_0$  can be estimated as follows:

$$V_c = V_0 - R_0 I_c \quad \text{D} \quad R_0 = \frac{(V_0 - V_c)}{I_c}. \quad (12)$$

### C. Identification and validation of Line Impedance

Figure 18 and Figure 19 show respectively the comparisons between the measured and numerical pantograph voltage  $V_c$  and collected current  $I_c$ . Comparing numerical and experimental results it is possible to adjust the value of the line equivalent resistivity  $\rho$  compensating the tolerances and approximations on data (typically no more than 5-10%).

508 It is possible to highlight how the matching between simulated results and experimental measurements is quite good even considering  
509 the simplicity of the proposed model, the tolerances on several parameters and unavailability of further experimental data. In particular,  
510 higher errors can be found in the zone where the train speed is lower; however, due to the presence of axle skidding in the experimental  
511 measurements, it is difficult to further refine those results without any other data sets.



512

513 *Figure 19: Comparison between the collected current  $I_c$  experimentally measured at the pantograph during the traction phase and the corresponding*  
514 *numerical values obtained with the proposed model.*

515

#### 516 D. Feasibility of the Application of Energy Storage Systems to a High-speed Train

517 After the model experimental validation, the authors performed a set of simulations in order to investigate the feasibility of energy  
518 storage systems within the considered high-speed railway application. The proposed model has been used to analyse a series of different  
519 operating scenarios, all of them considering the same line (i.e. the “Direttissima” Firenze-Roma). The velocity profile considered for  
520 this feasibility analysis includes a first acceleration (applying the maximum traction effort) from standstill to 70 m/s, a constant speed  
521 phase and a final braking (considering, as a blending strategy, the maximization of the electrical converted power). In this operating  
522 scenario, the peak power involved in the braking phase is about 4-5 MW.

523 A previous analysis performed by the authors showed that, for high-speed railway application, the use of on-board storage devices is  
524 not useful: in fact, since the braking frequency is low but the involved energies are relatively high, the storage device should quite big

to be able to manage it, hence it would strongly affects the train loading capacity. Thus, in this research paper, only the results referred to the use of stationary storage devices are shown.

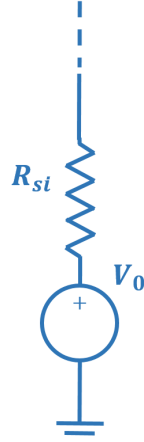


Figure 20: Scheme of the fully reversible sub-station.

#### E. Feasibility analysis

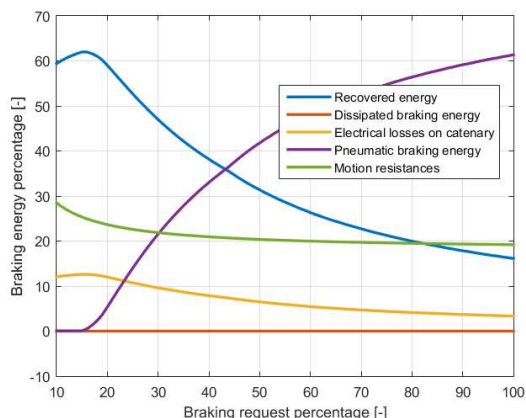
Since the results obtained through the simulation of the proposed model could be influenced by the particular behaviour or features of the considered energy storage device, the authors preferred to refer the numerical results to an ideal configuration in which the storage device has a near to infinite capacity ( $E=const$ ) and its no-load voltage is equal to  $V_0$  (i.e. no unbalance with respect to ESSs). As a further simplifying hypothesis it has been assumed that the equivalent impedances of both the ESSs and the coupled energy storage devices are equal to  $R_{si}$ . Under these hypotheses, the coupled ESS-energy storage device system is equivalent to the fully reversible substation shown in Figure 20.

This approach has been adopted in order to easily evaluate the performance of the system regardless of the constraints dependent on the storage technology. Figure 21, Figure 22 and Figure 23 show the main quantities considered in this analysis; the results shown in those Figures are all referred to scenarios where the braking manoeuvre starts at midspan between two adjacent ESSs, while the influence of the braking position is reported in Figure 24.

Figure 21 shows the energy fluxes involved in the train braking phase as functions of the braking request, which can be defined as follows:

$$Braking\ request = \frac{T_{B,desired}}{T_{B,nom}}, \quad (13)$$

543 where  $T_{B, nom}$  is the braking effort calculated according to the train performance characteristics (see Figure 2Figure ).

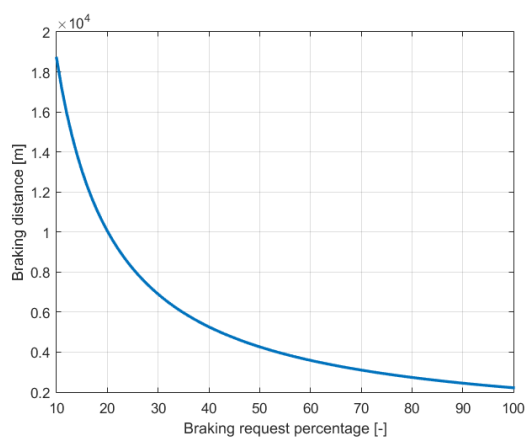


544

545 *Figure 21: Energy percentages involved in the train braking phase (measured at the pantograph) as a function of the braking effort percentage, without*  
546 *voltage limitations.*

547

548 By varying the braking request it is possible to vary the percentage of recovered energy since a higher braking request could saturate  
549 the braking effort and hence the braking energy.



550

551 *Figure 22: Braking distance as a function of the braking effort percentage, without voltage limitations.*

552 The recovered energy shows a maximum in correspondence of a 20% braking request; however, this low value of the braking request  
553 involves that the braking distance and the braking time (respectively reported in Figure 22 and Figure 23) are quite high, beyond the  
554 acceptable limits usually considered in high-speed applications. A good operating condition could be represented by the 50% braking



request, where about 30% of the braking energy can be recovered but the braking time and distance are acceptable. The braking energy dissipated on the on-board resistors is constantly 0 % since no voltage limiter is included in this first analysis.

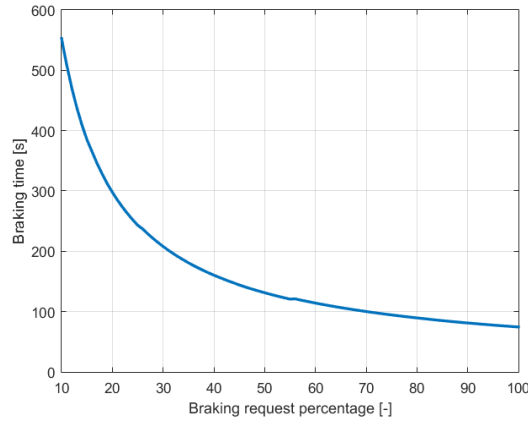


Figure 23: Braking time as a function of the braking effort percentage, without voltage limitations.

Figure 24 shows the voltage peak due to regenerative braking, as a function of the braking request and of the position between two adjacent Electrical Sub-Stations where the train begins the braking manoeuvre. According to Figure 6, the braking position between ESSs can be defined as follows:

$$\text{Braking position} = \frac{x}{l}. \quad (14)$$

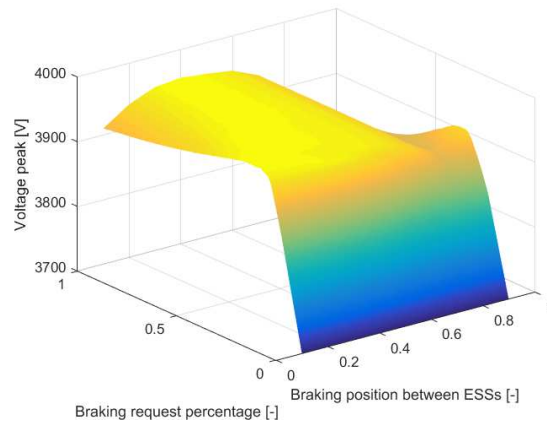
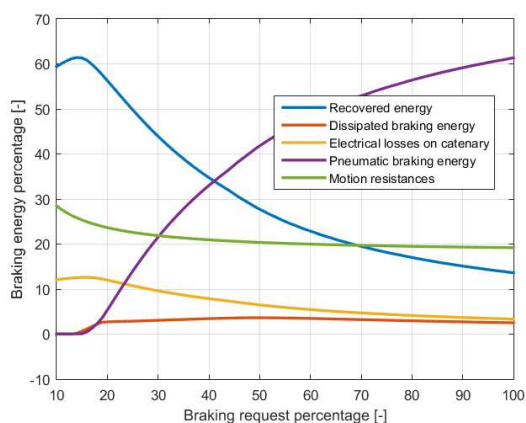


Figure 24: Line voltage peak during the braking phase as a function of the braking effort percentage and of the braking position between two adjacent Electrical Sub-Stations, without voltage limitations.

566 It is possible to highlight how the voltage peak, after a strong initial increase, is almost constant (or even decreasing) after the 20%  
567 braking request. On the contrary, the position where the braking phase begins has a significant influence on the voltage peak: it is  
568 possible to highlight how a braking manoeuvre that begins near a sub-station leads to lower voltage peaks on the line. This analysis  
569 could then be refined considering that usually trains are equipped with a proper device that cuts off regenerative braking (i.e. activates  
570 dissipative braking) if the voltage exceeds a certain value, which is about 3900 V; however, even this first analysis provides realistic  
571 results since the voltage peaks are not significantly higher with respect to the 3900 V limit.



572  
573 *Figure 25: Energy percentages involved in the train braking phase (measured at the pantograph) as a function of the braking effort percentage, voltage*  
574 *peak limited to 3900 V.*

575 Figure 25 and Figure 26 show the results obtained in terms of energy fluxes and voltage peaks using a voltage limiter (considering a  
576 limit value equal to 3900 V) during the braking phases. Figure 25 is essentially equal to Figure 21, since the voltage peak values obtained  
577 in absence of the voltage limiter were not significantly higher than the considered limit. However, it is possible to highlight how a small  
578 percentage of energy is dissipated on on-board resistors.

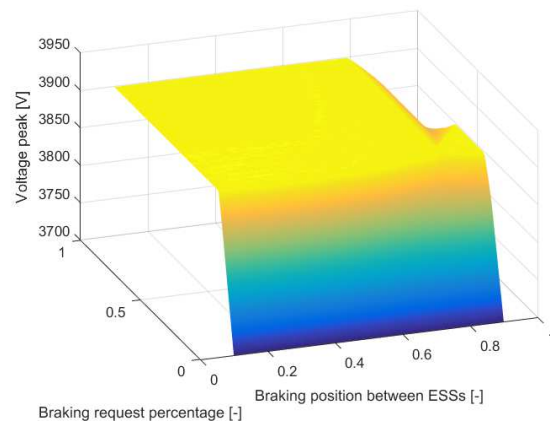


Figure 26: Line voltage peak during the braking phase as a function of the braking effort percentage and of the braking position between two adjacent Electrical Sub-Stations, voltage peak limited to 3900 V.

Figure 26 allows highlighting the small difference between the two scenarios: in fact the voltage peaks are saturated to the limit value for most of the braking position values. The voltage peaks, analogously to those obtained in absence of voltage limiter, are below the limit only in proximity of the ESSs, where the storage device is able to completely handle the energy peak provided in correspondence of the braking phase.

Finally, as reported in Table 7 together with characteristics of the computer used for the simulations, the proposed model proved to be highly efficient from the computational point of view: the simulation of the traction manoeuvre used for the validation requires only 1 second of computational time, while a simulation of the complete line (250 km) requires 5 seconds.

Table 7: Machine features and computational times.

CPU	Intel CORE i7
Clock frequency	2.30 GHz
RAM memory	8 Gb
Operative system	Windows 10 – 64 bit
$\frac{\text{machine time [s]}}{\text{time to be simulated [s]}}$	$4 \times 10^{-4}$

592 IV. CONCLUSIONS

593 The ever increasing attention to the environment and to pollution problems connected with transportations is pushing towards the  
594 achievement of higher energetic efficiency in all the transport sectors. Railway is currently in a favourable position but in order to  
595 preserve its competitiveness, it is fundamental to further optimize the energetic efficiency in the entire railway sector. One of the possible  
596 way to reach this goal is the use of energy recovery systems, in order to regenerate the kinetic energy of the vehicle that otherwise is  
597 dissipated during the braking phases.

598 Energy recovery systems have been widely analysed considering their application in the light railway field; however, the possibility to  
599 apply energy recovery in high-speed train is a quite new research field. High-speed railway has different needs with respect to light  
600 railway; hence it is necessary to understand which practical solution could fit the energetic characteristics of the considered application.  
601 In this paper the authors developed a model for the analysis of the interactions between the vehicle longitudinal dynamics and the  
602 electrical line which can be used to analyse the effects due to the introduction in the system of stationary or on-board energy storage  
603 devices.

604 The model has been validated considering a set of experimental data referred to a traction manoeuvre of the Italian ETR 1000 in the  
605 Firenze-Roma line. The results obtained with the proposed model, which has been developed using an innovative object oriented  
606 language, proved to be really accurate; furthermore, the computational efficiency of the model is extremely high since it allows to  
607 analyse train operation in a line of about 250 km in a few seconds of simulation time. After the validation the model has been used in  
608 order to analyse the feasibility of energy storage systems in a high-speed railway application. From this analysis, the authors have found  
609 that the use of stationary energy storage devices, located in correspondence of the Electrical Sub-Stations, could allow significant  
610 savings even in a high-speed system, where the braking frequency is quite low: considering an acceptable braking request it is possible  
611 to recover almost one third of the energy involved in the train braking phase. Nowadays those results are widely acknowledged by  
612 professional operators of the sector.

613 This research activity will continue in order to improve both the model itself and the simulated scenarios: a more sophisticated  
614 management of the energy storage systems through power converters will be introduced and more complex scenarios involving multiple  
615 vehicles travelling on the same line will be analysed.

616

617 BIBLIOGRAPHIC REFERENCES

618[1] Kamal WA. Improving energy efficiency - The cost-effective way to mitigate global warming. Energy Conversion and Management 1997; 38-1, p. 39-59.

619[2] European Environment Office, tech. reports at [www.eea.europa.eu](http://www.eea.europa.eu).

620[3] Association of American Railroads tech reports at <https://www.aar.org>.

621[4] Fridell E, Björk A, Ferm M, Ekberg A. On-board measurements of particulate matter emissions from a passenger train. Proceedings of the Institution of Mechanical  
622 Engineers, Part F: Journal of Rail and Rapid Transit 2011; 225-1, p. 99-106.

623[5] TSI, technical specifications for interoperability. Available at the official site of ERA (European Railway Agency) [http://www.era.europa.eu/Core-  
624 Activities/Interoperability/Pages/TechnicalSpecifications.aspx](http://www.era.europa.eu/Core-Activities/Interoperability/Pages/TechnicalSpecifications.aspx).

625[6] Douglas H, Roberts C, Hillmansen S, Schmid F. An assessment of available measures to reduce traction energy use in railway networks. Energy Conversion and  
626 Management 2015; 106, December 2015, p. 1149-1165.

627[7] Bartłomiejczyk M, Połom M. Multiaspect measurement analysis of breaking energy recovery. Energy Conversion and Management 2016; 127, p. 35-42.

628[8] Abbasi S, Jansson A, Olander L, Olofsson U, Sellgren U. A pin-on-disc study of the rate of airborne wear particle emissions from railway braking materials. Wear 2012;  
629 284, p. 18-29.

630[9] Gehrig R, Hill M, Lienemann P, Zwicky CN, Bukowiecki N, Weingartner E, Baltensperger U, Buchmann B. Contribution of railway traffic to local PM10 concentrations  
631 in Switzerland. Atmospheric Environment 2007; 41-5, p. 923-933.

632[10] Salma I, Weidinger T, Maenhaut W. Time-resolved mass concentration, composition and sources of aerosol particles in a metropolitan underground railway station.  
633 Atmospheric Environment 2007; 41-37, p. 8391-8405.

634[11] Marr WW, Walsh WJ, Symons PC. Modeling battery performance in electric vehicle applications. Energy Conversion and Management 1992; 33-9, p. 843-847.

635[12] Hillmansen S, Roberts C. Energy storage devices in hybrid railway vehicles: a kinematic analysis. Proceedings of the Institution of Mechanical Engineers, Part F: Journal  
636 of Rail and Rapid Transit 2007; 221-1, p. 135-143.

637[13] Peña-Alcaraz M, Fernández A, Cucala AP, Ramos A, Pecharromán RR. Optimal underground timetable design based on power flow for maximizing the use of  
638 regenerative-braking energy. Proceedings of the Institution of Mechanical Engineers, Part F: Journal of Rail and Rapid Transit 2012; 226-4, p. 397-408.

639[14] Falvo MC, Sbordone D, Fernández-Cardador A, Cucala AP, Pecharromán RR, López- López A. Energy savings in metro-transit systems: A comparison between  
640 operational Italian and Spanish lines. Proceedings of the Institution of Mechanical Engineers, Part F: Journal of Rail and Rapid Transit 2016; 230-2, p. 345-359.

641[15] González-Gil A, Palacin R, Batty P. Optimal energy management of urban rail systems: Key performance indicators. Energy Conversion and Management 2015; 90, p.  
642 282-291.

643[16] Barrero R, Tackoen X, Mierlo J. Stationary or onboard energy storage systems for energy consumption reduction in a metro network. Proceedings of the Institution of  
644 Mechanical Engineers, Part F: Journal of Rail and Rapid Transit 2010; 224, p. 207-225.

645[17] Teymourfar R, Asaei B, Iman-Eini H, Nejati Fard R. Stationary super-capacitor energy storage system to save regenerative braking energy in a metro line. Energy  
646 Conversion and Management 2012; 56, p. 206-214.

647[18] Teymourfar R, Nejati Fard R, Asaei B, Iman-Eini H. Energy recovery in a metro network using stationary supercapacitors. Power Electronics, Drive Systems and  
648 Technologies Conference (PEDSTC) 2011.

649[19] Ceraolo M, Lutzemberger G. Stationary and on-board storage systems to enhance energy and cost efficiency of tramways. *Journal of Power Sources* 2014; 264, p. 128-  
650 139.

651[20] Barrero R, Tackoen X, Van Mierlo J. Quasi-static simulation method for evaluation of energy consumption in hybrid light rail vehicles. *IEEE Vehicle Power and*  
652 *Propulsion Conference*. IEEE 2008.

653[21] Barrero R, Van Mierlo J, Tackoen X. Energy savings in public transport. *Vehicular Technology Magazine* 2008; 3-3, p.26-36.

654[22] Barrero R, Tackoen X, Van Mierlo J. Analysis and configuration of supercapacitor based energy storage system on-board light rail vehicles. *IEEE Power Electronics and*  
655 *Motion Control Conference*, 2008. EPE-PEMC 2008.

656[23] Van Mierlo J, Barrero R, Tackoen X. Supercapacitors On-Board Light Rail Vehicles: Enhanced Energy Storage Systems for Improved Vehicle Efficiency.  
657 *IEEE/ASME/ASCE 2008 Joint Rail Conference* 2008.

658[24] González-Gil A, Palacin R, Batty P. Sustainable urban rail systems: Strategies and technologies for optimal management of regenerative braking energy. *Energy*  
659 *Conversion and Management* 2013; 75, p. 374-388.

660[25] González-Gil A, Palacin R, Batty P, Powell JP. A systems approach to reduce urban rail energy consumption. *Energy Conversion and Management* 2014; 80, p. 509-  
661 524.

662[26] Iannuzzi D, Lauria D, Ciccirelli F. Wayside ultracapacitors storage design for light transportation systems: a multiobjective optimization approach. *International Review*  
663 *of Electrical Engineering (IREE)* 2013; 8-1, p. 190-199.

664[27] Mir L, Exteberria-Otadui I, Perez de Arenaza I, Sarasola I, Nieva T. A supercapacitor based light rail vehicle: system design and operations modes. *IEEE Energy*  
665 *Conversion Congress and Exposition* 2009.

666[28] Vasebi A, Bathae SMT, Partovibakhsh M. Predicting state of charge of lead-acid batteries for hybrid electric vehicles by extended Kalman filter. *Energy Conversion*  
667 *and Management* 2008; 49-1, p. 75-82.

668[29] Tsang KM, Sun L, Chan WL. Identification and modelling of Lithium ion battery. *Energy Conversion and Management* 2010; 51-12, p. 2857-2862.

669[30] Castano S, Gauchia L, Voncila E, Sanz J. Dynamical modeling procedure of a Li-ion battery pack suitable for real-time applications. *Energy Conversion and Management*  
670 2015; 92, p. 396-405.

671[31] Zhu WH, Zhu Y, Tatarchuk BJ. A simplified equivalent circuit model for simulation of Pb-acid batteries at load for energy storage application. *Energy Conversion and*  
672 *Management* 2011; 52-8, p. 2794-2799.

673[32] Trovão JP, Antunes CH. A comparative analysis of meta-heuristic methods for power management of a dual energy storage system for electric vehicles. *Energy*  
674 *Conversion and Management*, 2015; 95, p. 281-296.

675[33] Guo L, Yedavalli K, Zinger D. Design and modeling of power system for a fuel cell hybrid switcher locomotive. *Energy conversion and management* 2011; 52-2, p.  
676 1406-1413.

677[34] Paladini V, Donateo T, De Risi A, Laforgia D. Super-capacitors fuel-cell hybrid electric vehicle optimization and control strategy development. *Energy Conversion and*  
678 *Management* 2007; 48-11, p. 3001-3008.

679[35] Thiounn-Guermeur M. Evaluation of the hybrid locomotive PLATHEE - A Platform for Energy Efficiency and Environmentally Friendly Hybrid Trains. Proceeding of  
680 WCRR (World Congress of Railway Research), France, 2011.

681[36] Sharma P, Bhatti TS. A review on electrochemical double-layer capacitors. Energy Conversion and Management 2010; 51-12, p. 2901-2912.

682[37] Steiner M, Klohr M, Pagiela S. Energy storage system with ultracaps on board of railway vehicles. Power Electronics and Applications European Conference 2001; p.1-  
683 10.

684[38] Kondoh J, Ishii I, Yamaguchi H, Murata A, Otani K, Sakuta K, Higuchi N, Sekine S, Kamimoto M. Electrical energy storage systems for energy networks. Energy  
685 Conversion and Management 2000; 41-17, p. 1863-1874.

686[39] Fernão Pires V, Romero-Cadaval E, Vinnikov D, Roasto I, Martins JF. Power converter interfaces for electrochemical energy storage systems – A review. Energy  
687 Conversion and Management 2014; 86, p. 453-475.

688[40] Oliveira L, Messagie M, Mertens J, Laget H, Coosemans T, Van Mierlo J. Environmental performance of electricity storage systems for grid applications, a life cycle  
689 approach. Energy Conversion and Management 2015; 101, p. 326-335.

690[41] Fernandez LM, Garcia P, Garcia CA, Jurado F. Hybrid electric system based on fuel cell and battery and integrating a single dc/dc converter for a tramway. Energy  
691 Conversion and Management 2011; 52-5, p. 2183-2192.

692[42] Uzunoglu M, Alam MS. Dynamic modeling, design and simulation of a PEM fuel cell/ultra-capacitor hybrid system for vehicular applications. Energy Conversion and  
693 Management 2007; 48-5, p. 1544-1553.

694[43] Hannan MA, Azidin FA, Mohamed A. Multi-sources model and control algorithm of an energy management system for light electric vehicles. Energy Conversion and  
695 Management 2012; 62, p. 123-130.

696[44] Pugi L, Conti R, Nocciolini D, Galardi E, Meli E. A Comprehensive Tool for the Optimization of Traction and Braking systems with respect to the Application of Energy  
697 Storage Devices. International Journal of Railway Technology 2015; 4, p. 69-93.

698[45] Conti R, Galardi E, Meli E, Nocciolini D, Pugi L, Rindi A. Energy and wear optimisation of train longitudinal dynamics and of traction and braking systems. Vehicle  
699 System Dynamics 2015; p. 1-22.

700[46] Ramakrishnan R, Hiremath SS, Singaperumal M. Dynamic Analysis and Design Optimization of Series Hydraulic Hybrid System through Power Bond Graph Approach.  
701 International Journal of Vehicular Technology 2014.

702[47] Allotta B, Pugi L. Meccatronica: Elementi di Trazione Elettrica. 1st ed. Bologna: Esculapio Editore; 2013.

703[48] Leigh MJ. Brake blending. Proceedings of the Institution of Mechanical Engineers, Part F: Journal of Rail and Rapid Transit 1994; 208-1, p. 43-49.

704[49] Perticaroli F. Sistemi Elettrici per i Trasporti. Rozzano: Casa Editrice Ambrosiana; 2001.

705[50] Zaninelli D., Sistemi elettrici per l'alta velocità ferroviaria. Milano: Hoepli; 2011.

706[51] Cornic D. Efficient recovery of braking energy through a reversible dc substation. Electrical Systems for Aircraft, Railway and Ship Propulsion 2010.

707[52] ETR1000 – Technical specifications. ansaldobreda.it. (original web page currently discontinued by Hitachi Rail after the acquisition of AnsaldoBreda).

708[53] Gherardi F, Vannelli L. The European interoperability and the related engineering and certification challenges. ZEV rail Glasers Annalen 2013; 137, p. 188-195.

709[54] L'evoluzione del sistema AV e il Frecciarossa 1000. CIFI Symposium, 1<sup>st</sup> July 2015; Proceedings available at [http://www.cifi.it/UpIDocumenti/AV\\_Freccia1000.htm](http://www.cifi.it/UpIDocumenti/AV_Freccia1000.htm).

- 710[55] Zhang X, Zhang Z, Pan H, Salman W, Yuan Y, Liu Y. A portable high-efficiency electromagnetic energy harvesting system using supercapacitors for renewable energy  
711 applications in railroads. *Energy Conversion and Management* 2016; 118, p. 287-294.
- 712[56] Chau K T, Wong YS. Overview of power management in hybrid electric vehicles. *Energy conversion and management* 2002; 43-15, p. 1953-1968.
- 713[57] Vinot E, Trigui R. Optimal energy management of HEVs with hybrid storage system. *Energy Conversion and Management* 2013; 76, p. 437-452.
- 714[58] Katrašnik T. Analytical framework for analyzing the energy conversion efficiency of different hybrid electric vehicle topologies. *Energy Conversion and Management*  
715 2009; 50-8, p. 1924-1938.
- 716[59] Ayad MY, Pierfederici S, Raël S, Davat B. Voltage regulated hybrid DC power source using supercapacitors as energy storage device. *Energy Conversion and*  
717 *Management* 2007; 48-7, p. 2196-2202.